Dynamics of an unbalanced two-ion crystal in a Penning trap for application in optical mass spectrometry

M. J. Gutiérrez,[1,*] J. Berrocal,[1] F. Domínguez,[1] I. Arrazola,[2] M. Block,[3,4,5] E. Solano,[2,6,7] and D. Rodríguez[1,8,†]

[1]*Departamento de Física Atómica, Molecular y Nuclear, Universidad de Granada, 18071 Granada, Spain*

[2]*Department of Physical Chemistry, University of the Basque Country UPV/EHU, Apartado 644, E-48080 Bilbao, Spain*

[3]*Institut für Kernchemie, Johannes Gutenberg-Universität Mainz, D-55099 Mainz, Germany*

[4]*GSI Helmholtzzentrum für Schwerionenforschung GmbH, D-64291 Darmstadt, Germany*

[5]*Helmholtz-Institut Mainz, D-55099 Mainz, Germany*

[6]*IKERBASQUE, Basque Foundation for Science, Maria Diaz de Haro 3, E-48013 Bilbao, Spain*

[7]*International Center of Quantum Artificial Intelligence for Science and Technology (QuArtist) and Department of Physics, Shanghai University, 200444 Shanghai, China*

[8]*Centro de Investigación en Tecnologías de la Información y las Comunicaciones, Universidad de Granada, 18071 Granada, Spain*

(Received 14 June 2019; revised manuscript received 11 September 2019; published 10 December 2019)

In this paper, the dynamics of an unbalanced two-ion crystal comprising the "target" and the "sensor" ions confined in a Penning trap along the magnetic-field axis has been studied. First, the low amplitude regime is addressed. In this regime, the overall potential including the Coulomb repulsion between the ions can be considered harmonic and the axial, magnetron, and reduced-cyclotron modes split up into the so-called stretch and common modes, that are generalizations of the well-known "breathing" and "center-of-mass" motions of a balanced crystal made of two ions. By using optical detection to measure the frequencies of the modes of the crystal, and of the sensor ion on its own, in the quantum regime of motion, it will be possible to determine the target ion's free-cyclotron frequency. The nonharmonicity of the Coulomb interaction is also discussed since this causes large systematic effects, which are minimized due to the high sensitivity of the optical detection method when the crystal is cooled to the ground state of motion in the Penning trap.

DOI: 10.1103/PhysRevA.100.063415

I. INTRODUCTION

A precise determination of atomic and nuclear masses of exotic particles is of fundamental interest in many areas, for example, in nuclear physics and in neutrino physics [1,2]. The determination of nuclear binding energies of exotic nuclides has contributed to a better understanding of their nuclear structure by identifying the changes in shell structure or by finding the onset of deformation (see, e.g., [3]). Superheavy elements (SHEs) are among the most challenging objects for such investigations since they can only be produced in quantities of a few atoms at a time in only four facilities worldwide, and they are often short lived [4–8]. Among these large-scale facilities, there is just one Penning trap system, at GSI-Darmstadt [9], which allows direct mass measurements by means of Penning traps [10]. However, the minute production yields for SHEs ($Z \geqslant 104$) call for measurement techniques of utmost sensitivity, capable of characterizing isotopes over a wide mass range using a single ion. In addition, in the case of a nondestructive measurement technique, additional observables such as nuclear decay modes and half-lives can be obtained from the very same ion. Such an approach would also benefit precise mass measurements that are required in the context of neutrino physics where often the mass of rare isotopes, available only in limited samples, is demanded. The limitation in sensitivity of the phase-imaging ion-cyclotron-resonance (PI-ICR) technique, currently in use at GSI-Darmstadt, to about ten ions [11] motivated the development of new techniques [12,13]. Developments for single-ion sensitivity on rare ions, using electronic detection, are also ongoing at the National Superconducting Cyclotron Laboratory [14].

In this paper, we present the results from analytical calculations of the dynamics of an unbalanced two-ion crystal in a 7-T Penning trap [15]. The outcomes from the calculations can be combined with the optical response of the sensor ion after applying external fields in resonance with the motional modes of the crystal. The proposed method is universal (with respect to the mass-to-charge ratio), and offers a permanent monitoring of the motion of the sensor ion in the trap. Although masses of some stable ions have been measured with relative uncertainties on the order of 10^{-10} to 10^{-11} by means of techniques based on electronic detection (see, e.g., a recent review in [16]), in all those cases, the ions are generated by off-line sources, inside the trap, or outside with large electronic charge states. Using optical detection, we aim at improving sensitivity, reaching a competitive level of accuracy for nuclear physics studies in a first stage, and with prospects to contribute to the determination of the mass of the electron antineutrino, the latter, for example, by performing mass measurements on $^{187}Re^{+}$ and $^{187}Os^{+}$, the masses of which have been already improved using a Penning trap technique developed for rare isotopes [11,17].

*mjgutierrez@ugr.es; this work is part of the Ph.D. thesis of M. J. Gutiérrez.

†danielrodriguez@ugr.es

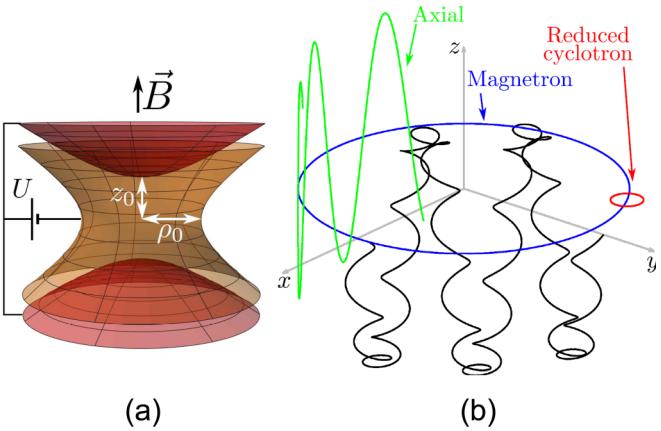

FIG. 1. Left: Original shape of a Penning trap (revolution hyperboloid). The yellow electrode is referred to as the *ring*, and the red ones are known as *endcaps*. The so-called *characteristic distance* of the trap is given by $d_0^2 = (z_0^2 + \rho_0^2/2)/2$. Right: Normal modes of a single ion stored in a Penning trap. The black solid line depicts the overall motion.

II. PENNING TRAP DYNAMICS

A Penning trap (see the left panel of Fig. 1) uses the combined effect of a strong homogeneous magnetic field, $\vec{B} = B\hat{z}$, and a quadrupolar electrostatic field, $V = (U/4d_0^2)(2z^2 - x^2 - y^2)$, to confine a charged particle or a crystal [18]. In this section the dynamics of the unbalanced two-ion crystal in a Penning trap is presented, after introducing the dynamics of the single trapped ion and obtaining the general equations in the low amplitude regime. Solving these equations numerically for a particular case allows characterization of the frequency shifts arising from the nonharmonic nature of the Coulomb repulsion. Previous work on ion crystals formed by identical ions stored in the same Penning trap has been carried out at Imperial College [19,20], while ultraaccurate mass spectrometry using two different ions stored simultaneously in a large magnetron orbit, to minimize their electrostatic interaction, was developed at Massachusetts Institute of Technology [21,22]. This Penning trap was relocated afterwards to Florida State University [23]. There, an additional Penning trap technique [24], based on work of the Harvard group [25], was used.

The motion of a single ion confined in an ideal Penning trap is well known [18]. The only force with a nonzero projection along the revolution axis is that of the electrostatic field. Since the field is quadrupolar, the resulting motion is harmonic with an oscillation frequency

$$\omega_z = 2\pi\nu_z = \sqrt{\frac{qU}{md_0^2}}. \tag{1}$$

The motion in the radial plane is an epicyclic orbit with frequencies

$$\nu_{c'/m} = \frac{\nu_c}{2}\left[1 \pm \sqrt{1 - 2\left(\frac{\nu_z}{\nu_c}\right)^2}\right]. \tag{2}$$

The subscript c' (corresponding to the $+$ sign) is associated to the so-called reduced-cyclotron motion, the frequency of which is very close to the free cyclotron frequency of the ion in the magnetic field, $\omega_c = 2\pi\nu_c = qB/m$. The subscript m, on the other hand, corresponds to the magnetron motion, the frequency of which is much lower than all the other involved frequencies under normal operation conditions.

The relationship between ν_c and the ion's mass depends only on the magnetic field, thus the precise determination of ν_c is the most common way to perform high-precision mass measurements. Since the ions do not oscillate with this frequency, relationships between the motional frequencies and the true cyclotron frequency are utilized, namely,

$$\nu_c = \nu_{c'} + \nu_m \tag{3}$$

and

$$\nu_c^2 = \nu_{c'}^2 + \nu_z^2 + \nu_m^2. \tag{4}$$

These can be easily derived from Eq. (2). The latter involves the measurement of an additional eigenfrequency, ν_z. However, it provides an advantage: Eq. (4), known as the *invariance theorem*, holds for *real* Penning traps [26], i.e., traps with a small misalignment between electric and magnetic field or with electric-field imperfections.

In a crystal made of two different ions, one defines the mass ratio $\mu = m_t/m_s$, where the subscript t denotes the "target" ion or "ion of interest" and s denotes the "sensor" ion. The axial and cyclotron frequencies of the target ion are $\omega_{zt} = \omega_0/\sqrt{\mu}$ and $\omega_{ct} = \omega_{cs}/\mu$, respectively, with ω_0 and ω_{cs} being the axial and true cyclotron frequency of the sensor ion. The orientation of the crystal can be axial or radial. This depends on frequency ratios. For example, if the crystal is composed of two identical ions, the axial orientation is energetically favorable provided [19]

$$\omega_z^2 < \tfrac{1}{6}\omega_c^2. \tag{5}$$

In this direction the distance between the ions in equilibrium is fixed.

In order to solve the equations for the unbalanced crystal (Appendix A), we will work in the small amplitude regime, i.e., when the displacement from the equilibrium position is $\ll d$, d being the distance between the target and sensor ion along the z axis in the equilibrium position (see Fig. 2). Under these conditions, the Coulomb interaction can be considered harmonic. In this case the Coulomb force is Taylor expanded to first order and the resulting equations are

$$\begin{aligned}
\ddot{x}_t &= \frac{1}{\mu}\omega_0^2 x_t + \frac{1}{\mu}\omega_{cs}\dot{y}_t - \frac{1}{2}\frac{1}{\mu}\omega_0^2 x_s,\\
\ddot{y}_t &= \frac{1}{\mu}\omega_0^2 y_t - \frac{1}{\mu}\omega_{cs}\dot{x}_t - \frac{1}{2}\frac{1}{\mu}\omega_0^2 y_s,\\
\ddot{z}_t &= -2\frac{1}{\mu}\omega_0^2 z_t + \frac{1}{\mu}\omega_0^2 z_s,\\
\ddot{x}_s &= \omega_0^2 x_s + \omega_{cs}\dot{y}_s - \frac{1}{2}\omega_0^2 x_t,\\
\ddot{y}_s &= \omega_0^2 y_s - \omega_{cs}\dot{x}_s - \frac{1}{2}\omega_0^2 y_t,\\
\ddot{z}_s &= -2\omega_0^2 z_s + \omega_0^2 z_t.
\end{aligned} \tag{6}$$

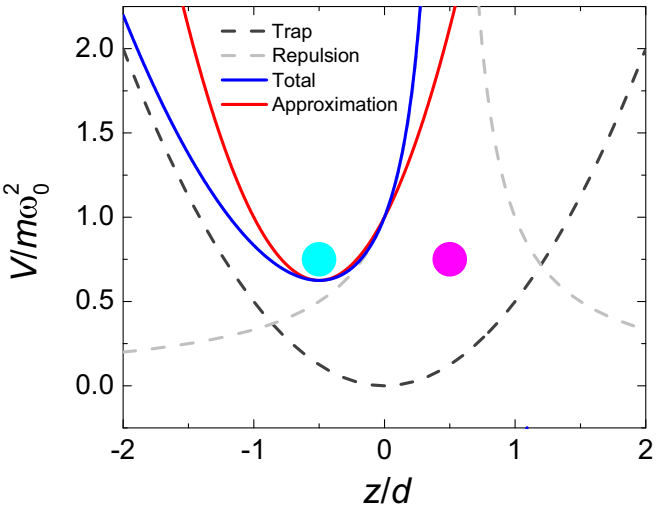

FIG. 2. Electric potentials as seen by the ion at $z = -d/2$ (colored in cyan) along the trap axis. The repulsion term is due to the presence of a second (pink-colored) ion.

In this approximation, the coupling between radial and axial motions disappears, and thus the equations in the radial plane and axial direction can be solved separately.

A. Axial motion

The equations describing the axial motion can be written in matrix form as

$$\begin{pmatrix} \ddot{z}_t \\ \ddot{z}_s \end{pmatrix} = \omega_0^2 \begin{pmatrix} \frac{-2}{\mu} & \frac{1}{\mu} \\ 1 & -2 \end{pmatrix} \begin{pmatrix} z_t \\ z_s \end{pmatrix}. \tag{7}$$

The normal modes and frequencies are obtained by diagonalizing the coefficient matrix, yielding

$$\ddot{Z}_\pm = -(\Omega_z^\pm)^2 Z_\pm, \ (\Omega_z^\pm)^2 = \omega_0^2 \left[1 + \frac{1}{\mu} \pm \sqrt{1 + \frac{1}{\mu^2} - \frac{1}{\mu}} \right]. \tag{8}$$

Here, + and − stand for *stretch* and *common* mode, respectively. They are related to the amplitudes of the ions by

$$Z_\pm = \left(1 - \frac{1}{\mu} \mp \sqrt{1 + \frac{1}{\mu^2} - \frac{1}{\mu}} \right) z_t + z_s, \tag{9}$$

where a global normalization factor has been omitted. Thus, the ions move in phase for the common mode, and out of phase for the stretch mode. The lighter ion moves with more amplitude than the heavier one in this mode, and with less amplitude in the common one as shown in Fig. 3. These results naturally agree with those obtained using a Paul trap [27].

B. Radial motion

The radial part of Eq. (6) can be written as

$$\begin{aligned} \begin{pmatrix} \ddot{u}_t \\ \ddot{u}_s \end{pmatrix} &= -i\omega_{cs} \begin{pmatrix} \frac{1}{\mu} & 0 \\ 0 & 1 \end{pmatrix} \begin{pmatrix} \dot{u}_t \\ \dot{u}_s \end{pmatrix} + \omega_0^2 \begin{pmatrix} \frac{1}{\mu} & -\frac{1}{2}\frac{1}{\mu} \\ -\frac{1}{2} & 1 \end{pmatrix} \begin{pmatrix} u_t \\ u_s \end{pmatrix} \\ &= M_{\rm dot} \begin{pmatrix} \dot{u}_t \\ \dot{u}_s \end{pmatrix} + M \begin{pmatrix} u_t \\ u_s \end{pmatrix} \end{aligned} \tag{10}$$

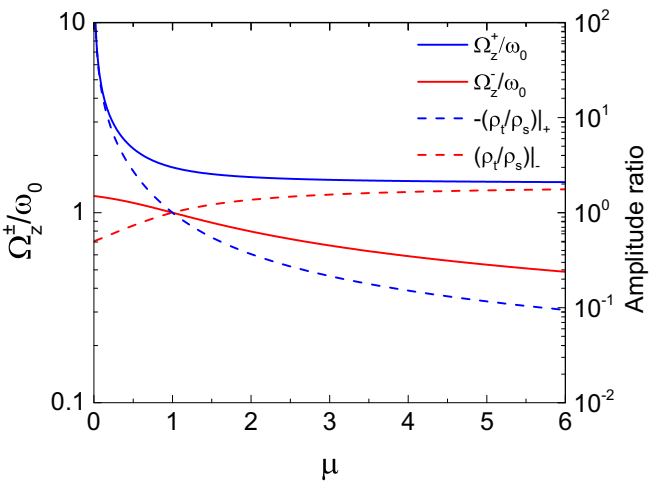

FIG. 3. Eigenvalues and eigenvectors for the two-ion crystal in the axial degree of freedom. The solid lines correspond to the axial frequencies in units of the axial frequency of the sensor ion. Note that the *stretch* frequency is almost constant for large values of μ; the same happens for the *common* mode when μ is small. The dashed lines correspond to the ions' amplitude ratios (target over sensor).

after the usual change of variable $u_{t,s} = x_{t,s} + iy_{t,s}$. The easiest way to find the normal modes and frequencies of the system is to find a base where M and $M_{\rm dot}$ are simultaneously diagonal, thus both matrices have to commute. However,

$$\begin{aligned} &\frac{i}{\omega_{cs}\omega_0^2}[M_{\rm dot}, M] \\ &\quad = \frac{1}{2}\frac{1}{\mu}(\mu - 1) \begin{pmatrix} 0 & -\frac{1}{\mu} \\ 1 & 0 \end{pmatrix} = 0 \Leftrightarrow \mu = 1. \end{aligned} \tag{11}$$

This implies that the radial motion can only be studied using this procedure when $\mu = 1$ (equal masses). Although this case is of no interest for mass spectrometry, its study gives insight on the motion of two simultaneously trapped ions. Diagonalizing M in Eq. (10) yields the eigenvalues

$$\Lambda_\pm = \omega_0^2 \frac{2 \pm 1}{2} \tag{12}$$

and eigenvectors

$$U_\pm = u_t \mp u_s. \tag{13}$$

U_- corresponds to a *center-of-mass* motion in the radial plane ($U_+ = 0 \Rightarrow u_t = u_s$). U_+, on the other hand, is a *breathing* motion ($U_- = 0 \Rightarrow u_t = -u_s$). Equation (10) can be written, in its diagonalized form, as

$$\begin{aligned} \ddot{U}_+ &= -i\omega_{cs}\dot{U}_+ + \frac{3}{2}\omega_0^2 U_+ = -i\omega_{cs}\dot{U}_+ + \Lambda_+ U_+, \\ \ddot{U}_- &= -i\omega_{cs}\dot{U}_- + \frac{1}{2}\omega_0^2 U_- = -i\omega_{cs}\dot{U}_- + \Lambda_- U_-. \end{aligned} \tag{14}$$

Each of these is equivalent to the equation of motion of a single ion, and can be solved to obtain the motional frequencies. These are, for the + mode,

$$\Omega_{c',m}^+ = \frac{\omega_{cs}}{2} \left[1 \pm \sqrt{1 - 2\left(\frac{\sqrt{3}\omega_0}{\omega_{cs}} \right)^2} \right]. \tag{15}$$

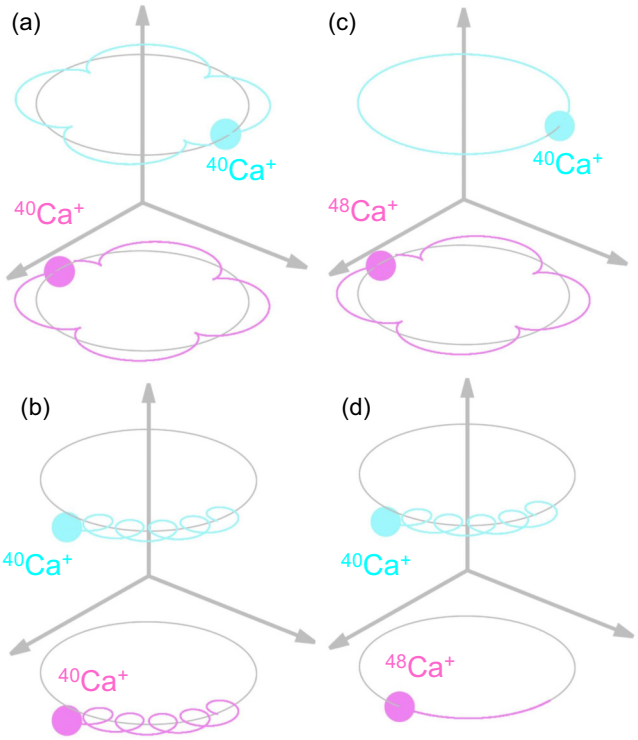

FIG. 4. (a) Balanced crystal moving in the breathing (magnetron and reduced-cyclotron) modes. (b) Balanced crystal moving in the center-of-mass modes. (c) Unbalanced crystal moving in the stretch mode (magnetron and reduced cyclotron). (d) Unbalanced crystal moving in the center-of-mass mode.

Again, the subscript c' corresponds to the $+$ sign in front of the square root, and the subscript m corresponds to the minus sign. Similarly, for the $-$ mode,

$$\Omega^{-}_{c',m} = \frac{\omega_{cs}}{2}\left[1 \pm \sqrt{1-2\left(\frac{\omega_0}{\omega_{cs}}\right)^2}\right], \tag{16}$$

which can be rewritten as

$$\Omega^{\pm}_{c',m} = \frac{\omega_{cs}}{2}\left[1 \pm \sqrt{1-2\left(\frac{\Omega^{\pm}_z}{\omega_{cs}}\right)^2}\right] \tag{17}$$

where $\Omega^{\pm}_z = \sqrt{2 \pm 1}\omega_0$ for two identical ions [Eq. (8)]. This equation is very similar to Eq. (2) and yields the radial frequencies of a balanced crystal as a function of the single-ion cyclotron frequency and the axial frequencies of the crystal. Figures 4(a) and 4(b) depict the radial motion of this crystal. The higher frequency for the reduced-cyclotron motion corresponds to the center-of-mass motion. This is different compared to the axial and magnetron motions, where the higher frequencies correspond to the breathing mode.

In the general case ($\mu \neq 1$) there are still two high-frequency (reduced-cyclotron) modes and two low-frequency (magnetron) modes [Figs. 4(c) and 4(d)]. For each of them there is an in-phase (common) mode and an opposite-phase (stretch) mode. In order to characterize them, the ansatz $u_{t,s} = \rho_{t,s}e^{-i\Omega t}$ is introduced into Eq. (10). By dividing over ω^2_{cs}, the

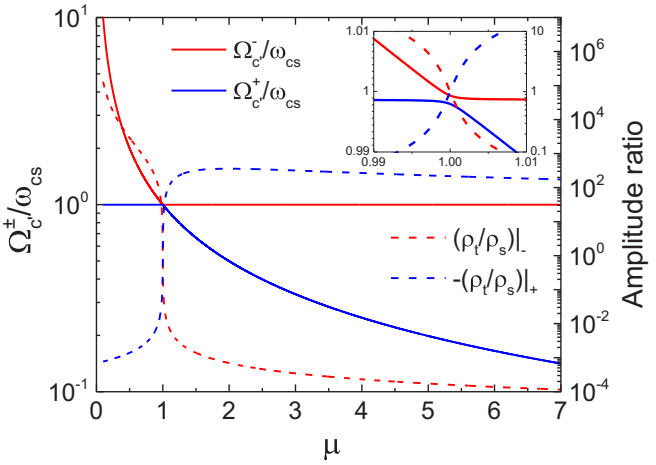

FIG. 5. Eigenvalues and eigenvectors of the reduced-cyclotron motion of the two-ion crystal. The solid lines correspond to the frequencies in units of the cyclotron frequency of the sensor ion ω_{cs}, whereas the dashed lines correspond to the amplitude ratios (target over sensor). The inset shows a zoomed-in version around $\mu = 1$.

resulting expression is

$$\left[\left(\frac{\Omega}{\omega_{cs}}\right)^2\begin{pmatrix}1 & 0\\ 0 & 1\end{pmatrix} - \frac{\Omega}{\omega_{cs}}\begin{pmatrix}\frac{1}{\mu} & 0\\ 0 & 1\end{pmatrix} + \left(\frac{\omega_0}{\omega_{cs}}\right)^2 \times \begin{pmatrix}\frac{1}{\mu} & -\frac{1}{2}\frac{1}{\mu}\\ -\frac{1}{2} & 1\end{pmatrix}\right]\begin{pmatrix}\rho_t\\ \rho_s\end{pmatrix} = 0, \tag{18}$$

which is known as a *nonlinear eigenproblem*. A numerical solution can be computed [28] to obtain the parameters of interest. The frequency ratio ω_0/ω_{cs} is the only trap-dependent quantity in the equation, as long as one solves it for Ω/ω_{cs}, which is the mode frequency normalized to the sensor ion's free cyclotron frequency. For our current trap configuration ($\omega_0/\omega_{cs} \simeq 0.0371$), the results are presented in Figs. 5 and 6. It is interesting to see that the reduced-cyclotron modes

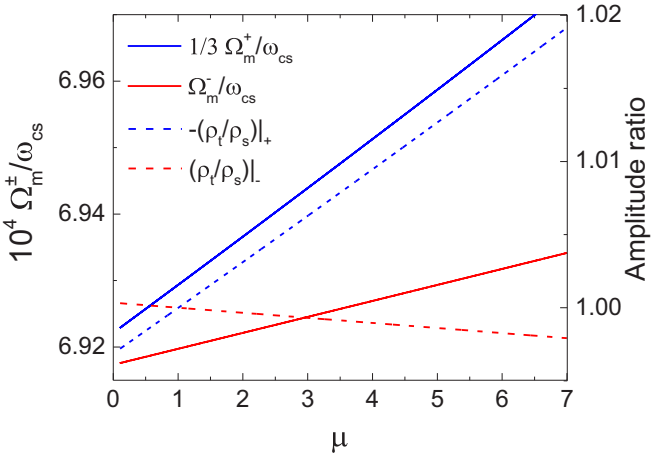

FIG. 6. Eigenvalues and eigenvectors of the magnetron motion of the two-ion crystal. The solid lines show the frequencies normalized to the cyclotron frequency of the sensor ion ω_{cs}. The dashed lines, on the other hand, show the amplitude ratios (target over sensor).

are weakly coupled (i.e., only one of the ions moves with significant amplitude) except for the region $\mu \sim 1$, where the frequencies are very similar. The motions can be considered perturbed versions of the individual reduced-cyclotron motions, where the most noticeable effect is an additional shift towards lower frequencies of about Ω_m^-. The magnetron motions remain strongly coupled. Higher values of the ratio ω_0/ω_{cs} (i.e., larger ion-ion coupling) result in larger magnetron frequencies (scaling with $\approx\omega_0^2$). Increasing the axial frequency, the region where the reduced-cyclotron modes have significant coupling extends further away from $\mu \sim 1$, and the $2\Omega_m^-$ deviation from the individual ions' free cyclotron frequencies still holds outside that mass interval.

III. MASS MEASUREMENTS WITH TWO TRAPPED IONS AND OPTICAL DETECTION

So far, calculations of the motional frequencies of a two-ion crystal as well as its dynamics have been shown. This allows determining the individual cyclotron frequencies for each of the ions forming the unbalanced crystal using a generalization of the invariance theorem [Eq. (4)] that reads [29,30]

$$\sum_{i=1}^{6} \omega_i^2 = \omega_{cs}^2 + \omega_{ct}^2, \tag{19}$$

where i is an index to account for each of the eigenfrequencies. The measurement of the crystal eigenfrequencies requires external fields applied in a similar way as it is done in many experiments [11,31–33]. However, the detection will differ, i.e., by using optical photons from the laser-cooled $^{40}Ca^+$ ion, instead of a micro-channel plate detector or via image charge detection with an electrical circuit. The cyclotron frequency of the sensor ion can be measured using the optical method on a single sensor ion stored in the trap and only cooled to the Doppler limit [34]. This measurement can be performed before and after the measurement of the crystal eigenmode frequencies. We also note that it is possible to know unequivocally whether a target ion has been produced and stored, since this results in a shift of the sensor ion's position of $d/2$ in the axial direction, that can be resolved by the CCD camera. This means that no produced ions are lost, as opposed to current techniques (time-of-flight ICR and PI-ICR), where the calibration measurements require isolating the traps from the incoming beam. In the following, the frequency shifts are calculated to analyze the applicability in optical mass spectrometry.

Up to this stage, our calculations were based on the low amplitude approximation [Eq. (6)]. However, when the oscillation amplitudes become large enough, some of the frequencies of the crystal modes shift with respect to the values given in Figs. 3, 5, and 6 (linear approximation). In order to characterize the frequency shifts for the six eigenmodes, we have calculated the 6×6 matrix, where each term is in units of hertz per phonon. The procedure described in [35] for ion crystals in a linear Paul trap has been followed but now adapting it to the Penning trap eigenmodes of an unbalanced crystal. The mathematical treatment is shown in Appendix B. Experimentally, the ion crystal should be cooled to its ground state of motion, which is possible by performing sideband cooling [36]. We calculate the tensors from Eqs. (B1) and (B2), as well as the matrix elements $e'_{\alpha,i}$ that connect the eigenmode basis with the ξ_i basis. The result for a $^{257}Rf^+$-$^{40}Ca^+$ crystal using the trap configuration $\omega_0/2\pi = 100$ kHz and $\omega_{cs}/2\pi = 2.689$ MHz is

$$\begin{pmatrix} \Delta\Omega_{c'}^- \\ \Delta\Omega_{c'}^+ \\ \Delta\Omega_m^+ \\ \Delta\Omega_m^- \\ \Delta\Omega_z^- \\ \Delta\Omega_z^+ \end{pmatrix} = 2\pi \times \begin{pmatrix} 0.0004 & 0.0016 & 0.3967 & 0.0000 & -0.0012 & -0.0162 \\ 0.0016 & 0.0004 & 0.4942 & 0.0000 & -0.0010 & -0.0124 \\ 0.3967 & 0.4942 & -0.4094 & -0.0003 & 2.0643 & -1.2477 \\ 0.0000 & 0.0000 & -0.0003 & -0.0000 & 0.0000 & 0.0000 \\ -0.0012 & -0.0010 & 2.0643 & 0.0000 & -0.0014 & 0.0172 \\ -0.0162 & -0.0124 & -1.2477 & 0.0000 & 0.0172 & 0.0469 \end{pmatrix} \begin{pmatrix} n_{c'}^- \\ n_{c'}^+ \\ n_m^+ \\ n_m^- \\ n_z^- \\ n_z^+ \end{pmatrix} \text{Hz}. \tag{20}$$

This dependence with the phonon number is linear in the quantum regime. After reaching the Doppler limit ($T \sim 1$ mK) the mean phonon number is given by $\langle n_\xi^\pm \rangle = k_B T/\hbar\Omega_\xi^\pm$, where k_B is Boltzmann's constant and $\hbar$ is Planck's constant over 2π. Only the common reduced-cyclotron eigenmode is in the quantum regime at this point with $\langle n_{c'}^- \rangle \simeq 10$. However, the system can in principle be cooled down to the ground state using similar techniques as developed for a single ion [36]. In this regime each of the eigenmodes can be excited individually to probe the frequencies. The dependence of their shifts as a function of the phonon number can be studied systematically. The readout can be done using a standard procedure as described in Ref. [37].

IV. CONCLUSIONS AND PERSPECTIVES

In this paper we have shown results from calculations of the dynamics of an unbalanced two-ion crystal for applications in optical Penning trap mass spectrometry. The significance of our method lies in the optical detection, which allows monitoring the sensor ion permanently in the trap. For small amplitudes, the Coulomb interaction can be considered harmonic. This has been studied in detail to obtain the eigenfrequencies and eigenvectors of the crystal. The frequency shifts shown in the 6×6 matrix [Eq. (20)] will prevent us from reaching high precision, if the crystal is not cooled to the ground state of motion. The highest dependence of the frequency shift of a mode as a function of phonon number in

the same mode appears in stretch axial and stretch magnetron modes, contributing to the relative uncertainty on the order of 10^{-8} per phonon in both cases. Here we rely on the feasibility of probing any of the modes preserving the phonon number of the remaining modes. In any case, these shifts can be taken into account in the measurement protocol as one can determine the number of phonons in each mode, so that the ultimate uncertainty is only limited by the precision achieved in the frequency measurement.

ACKNOWLEDGMENTS

M.J.G., J.B., F.D., M.B., and D.R. acknowledge support from the European Research Council (Contract No. 278648-TRAPSENSOR), from the Spanish MINECO (now MCIU) through Project No. FPA2015-67694-P, from the Spanish Ministry of Education through Ph.D. fellowships (Grants No. FPU15/04679 and No. FPU17/02596), from the University of Granada "Plan propio—Programa de Intensificación de la Investigación" Project No. PP2017-PRI.I-04, from infrastructure projects of MINECO/FEDER/Universidad de Granada (Projects No. UNGR10-1E-501 and No. UNGR13-1E-1830), and from Junta de Andalucía/FEDER Grant No. IE-5713. I.A. and E.S. acknowledge support from MCIU/AEI/FEDER,UE Grant No. PGC2018-095113-B-I00, from the Basque Government through Project No. IT986-16 and Ph.D. Grant No. PRE-2015-1-039 (I.A.), and from QMiCS Grant No. 820505 and OpenSuperQ Grant No. 820363 of the European Union (EU) Flagship on Quantum Technologies and EU FET Open Grant Quromorphic.

APPENDIX A: EQUATIONS OF MOTION

The equations of motion of two singly charged ions of masses m_t and m_s confined simultaneously in a Penning trap, using coordinates with respect to the trap center, can be written as

$$\begin{aligned}
\ddot{x}_t &= \frac{1}{\mu}\frac{\omega_0^2}{2}x_t + \frac{1}{\mu}\omega_{cs}\dot{y}_t + \frac{1}{m_t}\frac{e^2}{4\pi\varepsilon_0}\frac{(\vec{r}_t-\vec{r}_s)\cdot\hat{x}}{|\vec{r}_t-\vec{r}_s|^3},\\
\ddot{y}_t &= \frac{1}{\mu}\frac{\omega_0^2}{2}y_t - \frac{1}{\mu}\omega_{cs}\dot{x}_t + \frac{1}{m_t}\frac{e^2}{4\pi\varepsilon_0}\frac{(\vec{r}_t-\vec{r}_s)\cdot\hat{y}}{|\vec{r}_t-\vec{r}_s|^3},\\
\ddot{z}_t &= -\frac{1}{\mu}\omega_0^2 z_t + \frac{1}{m_t}\frac{e^2}{4\pi\varepsilon_0}\frac{(\vec{r}_t-\vec{r}_s)\cdot\hat{z}}{|\vec{r}_t-\vec{r}_s|^3},\\
\ddot{x}_s &= \frac{\omega_0^2}{2}x_s + \omega_{cs}\dot{y}_s - \frac{1}{m_s}\frac{e^2}{4\pi\varepsilon_0}\frac{(\vec{r}_t-\vec{r}_s)\cdot\hat{x}}{|\vec{r}_t-\vec{r}_s|^3},\\
\ddot{y}_s &= \frac{\omega_0^2}{2}y_s - \omega_{cs}\dot{x}_s - \frac{1}{m_s}\frac{e^2}{4\pi\varepsilon_0}\frac{(\vec{r}_t-\vec{r}_s)\cdot\hat{y}}{|\vec{r}_t-\vec{r}_s|^3},\\
\ddot{z}_s &= -\omega_0^2 z_s - \frac{1}{m_s}\frac{e^2}{4\pi\varepsilon_0}\frac{(\vec{r}_t-\vec{r}_s)\cdot\hat{z}}{|\vec{r}_t-\vec{r}_s|^3}.
\end{aligned} \tag{A1}$$

where $\mu = m_t/m_s$. The parameters $\omega_{zt} = \omega_0/\sqrt{\mu}$ and $\omega_{ct} = \omega_{cs}/\mu$ are the axial and true cyclotron frequencies of the target ion, respectively. ω_0 and ω_{cs} are the axial and true cyclotron frequencies of the sensor ion. The last term of each equation accounts for the Coulomb repulsion between the two ions.

In the case of an unbalanced crystal oriented in the axial direction (see Fig. 2), the equilibrium positions are $z_t^{\mathrm{eq}} = -z_s^{\mathrm{eq}} = d/2$, where $d^3 = e^2/(2\pi\varepsilon_0 m_s\omega_0^2)$ is the equilibrium distance. Referring the coordinates of each ion to its equilibrium position, the resulting equations are

$$\begin{aligned}
\ddot{x}_t &= \frac{1}{\mu}\frac{\omega_0^2}{2}x_t + \frac{1}{\mu}\omega_{cs}\dot{y}_t + \frac{\omega_0^2 d^3}{2}\frac{1}{\mu}\frac{(\vec{r}_t-\vec{r}_s+d\hat{z})\cdot\hat{x}}{|\vec{r}_t-\vec{r}_s+d\hat{z}|^3},\\
\ddot{y}_t &= \frac{1}{\mu}\frac{\omega_0^2}{2}y_t - \frac{1}{\mu}\omega_{cs}\dot{x}_t + \frac{\omega_0^2 d^3}{2}\frac{1}{\mu}\frac{(\vec{r}_t-\vec{r}_s+d\hat{z})\cdot\hat{y}}{|\vec{r}_t-\vec{r}_s+d\hat{z}|^3},\\
\ddot{z}_t &= -\frac{1}{\mu}\omega_0^2\left(z_t+\frac{d}{2}\right) + \frac{\omega_0^2 d^3}{2}\frac{1}{\mu}\frac{(\vec{r}_t-\vec{r}_s+d\hat{z})\cdot\hat{z}}{|\vec{r}_t-\vec{r}_s+d\hat{z}|^3},\\
\ddot{x}_s &= \frac{\omega_0^2}{2}x_s + \omega_{cs}\dot{y}_s - \frac{\omega_0^2 d^3}{2}\frac{(\vec{r}_t-\vec{r}_s+d\hat{z})\cdot\hat{x}}{|\vec{r}_t-\vec{r}_s+d\hat{z}|^3},\\
\ddot{y}_s &= \frac{\omega_0^2}{2}y_s - \omega_{cs}\dot{x}_s - \frac{\omega_0^2 d^3}{2}\frac{(\vec{r}_t-\vec{r}_s+d\hat{z})\cdot\hat{y}}{|\vec{r}_t-\vec{r}_s+d\hat{z}|^3},\\
\ddot{z}_s &= -\omega_0^2\left(z_s-\frac{d}{2}\right) - \frac{\omega_0^2 d^3}{2}\frac{(\vec{r}_t-\vec{r}_s+d\hat{z})\cdot\hat{z}}{|\vec{r}_t-\vec{r}_s+d\hat{z}|^3}.
\end{aligned} \tag{A2}$$

This system of equations can be partially solved for $\mu = 1$ (equal masses) for the center-of-mass motion, since the Coulomb term cancels out for $\Xi_{\mathrm{COM}} = \xi_t - \xi_s$, $\xi = \{x, y, x\}$. The resulting motion is the same as for the single ion.

APPENDIX B: CALCULATION OF FREQUENCY SHIFTS AT THE QUANTUM LEVEL

In order to calculate frequency shifts in the two-ion crystal it is convenient to change the original (Cartesian) coordinate system to a new system where $\xi_i' = \sqrt{m_i}\xi_i$. Here, $\xi_1 = x_t$, $\xi_2 = x_s$, $\xi_3 = y_t$, and so on, and m_i is the mass of the ion associated to the coordinate ξ_i. Expanding the Coulomb potential U to third and fourth order in this new basis (equivalent to second and third order in the Coulomb force, given that $\vec{F} = -\nabla U$) gives rise to the third- and fourth-order tensors $A'^{(3)}$ and $A'^{(4)}$, with elements

$$A'^{(3)}_{ijk} = \frac{1}{3!}\frac{1}{\sqrt{m_i m_j m_k}}\left.\frac{\partial^3 U}{\partial\xi_i\partial\xi_j\partial\xi_k}\right|_{\mathrm{eq}} \tag{B1}$$

and

$$A'^{(4)}_{ijkl} = \frac{1}{4!}\frac{1}{\sqrt{m_i m_j m_k m_l}}\left.\frac{\partial^4 U}{\partial\xi_i\partial\xi_j\partial\xi_k\partial\xi_l}\right|_{\mathrm{eq}}, \tag{B2}$$

taking into account that $\partial/\partial\xi_i' = (1/\sqrt{m_i})\partial/\partial\xi_i$. Therefore, the third- and fourth-order contributions to the potential are, respectively,

$$U^{(3)} = \sum_{i,j,k} A'^{(3)}_{ijk}\xi_i'\xi_j'\xi_k' \tag{B3}$$

and

$$U^{(4)} = \sum_{i,j,k,l} A'^{(4)}_{ijkl}\xi_i'\xi_j'\xi_k'\xi_l'. \tag{B4}$$

Now it is necessary to change to the eigenmode basis. This is done via the coefficients $e'_{\alpha,i}$, where the greek letter labels the mode and the latin letter labels the coordinate ξ_i:

$$G'^{(3)}_{\alpha\beta\gamma} = \sigma'_\alpha\sigma'_\beta\sigma'_\gamma\sum_{i,j,k} e'_{\alpha,i}e'_{\beta,j}e'_{\gamma,k}A'^{(3)}_{ijk}, \tag{B5}$$

$$G'^{(4)}_{\alpha\beta\gamma\delta} = \sigma'_\alpha\sigma'_\beta\sigma'_\gamma\sigma'_\delta \sum_{i,j,k,l} e'_{\alpha,i}e'_{\beta,j}e'_{\gamma,k}e'_{\delta,l}A'^{(4)}_{ijkl}. \tag{B6}$$

In these equations, $\sigma'_\alpha = \sqrt{\hbar/2\omega_\alpha}$.

Quantization of a harmonic oscillator in the coordinates $x' = \sqrt{m}x$ gives rise to the relationship $\hat{x}' = \sqrt{\hbar/2\omega}(\hat{a} + \hat{a}^\dagger)$, where $\hat{a}^\dagger$ and $\hat{a}$ are the creation and annihilation operators, respectively. Therefore, it is clear from the previous expressions that

$$\hat{U}^{(3)} = \sum_{\alpha,\beta,\gamma} G'^{(3)}_{\alpha\beta\gamma}(\hat{a}_\alpha + \hat{a}^\dagger_\alpha)(\hat{a}_\beta + \hat{a}^\dagger_\beta)(\hat{a}_\gamma + \hat{a}^\dagger_\gamma) \tag{B7}$$

and

$$\hat{U}^{(4)} = \sum_{\alpha,\beta,\gamma,\delta} G'^{(4)}_{\alpha\beta\gamma\delta}(\hat{a}_\alpha + \hat{a}^\dagger_\alpha)(\hat{a}_\beta + \hat{a}^\dagger_\beta)(\hat{a}_\gamma + \hat{a}^\dagger_\gamma)(\hat{a}_\delta + \hat{a}^\dagger_\delta). \tag{B8}$$

Due to symmetry reasons, $\hat{U}^{(3)}$ does not contribute in first-order perturbation theory. Therefore, the second-order contribution of $\hat{U}^{(3)}$, $\Delta E^{(2)}$, as well as the first-order contribution of $\hat{U}^{(4)}$, $\Delta E^{(1)}$, are required to consistently estimate the shift.

The energy shift in the $n_\zeta \to n_\zeta + 1$ transition (keeping all other phonon numbers constant) is [35]

$$\begin{aligned}
h\Delta f_\zeta(\{n_\alpha\}, n_\zeta) &= \Delta E^{(1)}(\{n_\alpha\}, n_\zeta + 1) - \Delta E^{(1)}(\{n_\alpha\}, n_\zeta) + \Delta E^{(2)}(\{n_\alpha\}, n_\zeta + 1) - \Delta E^{(2)}(\{n_\alpha\}, n_\zeta) \\
&= 12\left[(n_\zeta + 1)G'^{(4)}_{\zeta\zeta\zeta\zeta} + \sum_{\alpha\neq\zeta} G'^{(4)}_{\alpha\alpha\zeta\zeta}(2n_\alpha + 1)\right] \\
&\quad - \frac{36}{\hbar}\sum_{\alpha\neq\zeta}(2n_\alpha + 1)\left[\frac{2\omega_\alpha\left(G'^{(3)}_{\alpha\alpha\zeta}\right)^2}{4\omega_\alpha^2 - \omega_\zeta^2} + \frac{2\omega_\zeta\left(G'^{(3)}_{\zeta\zeta\alpha}\right)^2}{4\omega_\zeta^2 - \omega_\alpha^2} + \frac{G'^{(3)}_{\zeta\zeta\zeta}G'^{(3)}_{\alpha\alpha\zeta}}{\omega_\zeta} + \frac{G'^{(3)}_{\alpha\zeta\zeta}G'^{(3)}_{\alpha\alpha\alpha}}{\omega_\alpha}\right] \\
&\quad - \frac{6}{\hbar}(n_\zeta + 1)\left[10\frac{\left(G'^{(3)}_{\zeta\zeta\zeta}\right)^2}{\omega_\zeta} - 6\sum_{\alpha\neq\zeta}\frac{\left(G'^{(3)}_{\zeta\zeta\alpha}\right)^2\omega_\alpha}{4\omega_\zeta^2 - \omega_\alpha^2} + 12\sum_{\alpha\neq\zeta}\frac{\left(G'^{(3)}_{\alpha\zeta\zeta}\right)^2}{\omega_\alpha}\right] \\
&\quad - \frac{72}{\hbar}\sum_{\alpha\neq\zeta}\sum_{\beta\neq\alpha,\zeta}\left(G'^{(3)}_{\alpha\beta\zeta}\right)^2\left[\frac{(n_\alpha - n_\beta)(\omega_\beta - \omega_\alpha)}{(\omega_\beta - \omega_\alpha)^2 - \omega_\zeta^2} + \frac{(n_\alpha + n_\beta + 1)(\omega_\beta + \omega_\alpha)}{(\omega_\beta + \omega_\alpha)^2 - \omega_\zeta^2}\right] \\
&\quad - \frac{36}{\hbar}\sum_{\alpha\neq\zeta}\frac{G'^{(3)}_{\alpha\zeta\zeta}}{\omega_\alpha}\left[\sum_{\beta\neq\alpha,\zeta} G'^{(3)}_{\alpha\beta\beta}(2n_\beta + 1)\right].
\end{aligned} \tag{B9}$$

Derivating this equation with respect to a certain n_κ gives the element $S_{\zeta,\kappa}$ of a matrix that connects the frequency shift of a given mode with the phonon number of all modes:

$$h\begin{pmatrix}\Delta f_1\\ \Delta f_2\\ \cdots\\ \Delta f_6\end{pmatrix} = S\begin{pmatrix}n_1\\ n_2\\ \cdots\\ n_6\end{pmatrix}. \tag{B10}$$

The expression used for the diagonal terms is

$$S_{\zeta\zeta} = \frac{\partial(h\Delta f_\zeta)}{\partial n_\zeta} = 12G'^{(4)}_{\zeta\zeta\zeta\zeta} - \frac{6}{\hbar}\left[10\frac{\left(G'^{(3)}_{\zeta\zeta\zeta}\right)^2}{\omega_\zeta} - 6\sum_{\alpha\neq\zeta}\frac{\left(G'^{(3)}_{\zeta\zeta\alpha}\right)^2\omega_\alpha}{4\omega_\zeta^2 - \omega_\alpha^2} + 12\sum_{\alpha\neq\zeta}\frac{\left(G'^{(3)}_{\alpha\zeta\zeta}\right)^2}{\omega_\alpha}\right], \tag{B11}$$

and for the off-diagonal ones

$$\begin{aligned}
S_{\zeta\kappa} &= \frac{\partial(h\Delta f_\zeta)}{\partial n_\kappa} \\
&= 24G'^{(4)}_{\kappa\kappa\zeta\zeta} - \frac{72}{\hbar}\left[\frac{2\omega_\alpha\left(G'^{(3)}_{\kappa\kappa\zeta}\right)^2}{4\omega_\kappa^2 - \omega_\zeta^2} + \frac{2\omega_\zeta\left(G'^{(3)}_{\zeta\zeta\kappa}\right)^2}{4\omega_\zeta^2 - \omega_\kappa^2} + \frac{G'^{(3)}_{\zeta\zeta\zeta}G'^{(3)}_{\kappa\kappa\zeta}}{\omega_\zeta} + \frac{G'^{(3)}_{\kappa\zeta\zeta}G'^{(3)}_{\kappa\kappa\kappa}}{\omega_\kappa}\right. \\
&\quad \left. + \sum_{\alpha\neq\kappa,\zeta}\left[\left(G'^{(3)}_{\kappa\alpha\zeta}\right)^2 + \left(G'^{(3)}_{\alpha\kappa\zeta}\right)^2\right]\left(\frac{\omega_\alpha - \omega_\kappa}{(\omega_\alpha - \omega_\kappa)^2 - \omega_\zeta^2} + \frac{\omega_\alpha + \omega_\kappa}{(\omega_\alpha + \omega_\kappa)^2 - \omega_\zeta^2}\right) + \frac{G'^{(3)}_{\alpha\zeta\zeta}G'^{(3)}_{\alpha\kappa\kappa}}{\omega_\alpha}\right].
\end{aligned} \tag{B12}$$

[1] M. Block, D. Ackermann, K. Blaum, C. Droese, M. Dworschak, S. Eliseev, T. Fleckenstein, E. Haettner, F. Herfurth, F. P. Hessberger, S. Hofmann, J. Ketelaer, J. Ketter, H.-J. Kluge, G. Marx, M. Mazzocco, Y. N. Novikov, W. R. Plass, A. Popeko, S. Rahaman, D. Rodríguez, C. Scheidenberger, L. Schweikhard, P. G. Thirolf, G. K. Vorobyev, and C. Weber, Nature (London) **463**, 785 (2010).

[2] S. Eliseev, K. Blaum, M. Block, S. Chenmarev, H. Dorrer, C. E. Düllmann, C. Enss, P. E. Filianin, L. Gastaldo, M. Goncharov, U. Köster, F. Lautenschläger, Y. N. Novikov, A. Rischka, R. X. Schüssler, L. Schweikhard, and A. Türler, Phys. Rev. Lett. **115**, 062501 (2015).

[3] E. Minaya Ramirez, D. Ackermann, K. Blaum, M. Block, C. Droese, C. E. Düllmann, M. Dworschak, M. Eibach, S. Eliseev, E. Haettner, F. Herfurth, F. P. Heßberger, S. Hofmann, J. Ketelaer, G. Marx, M. Mazzocco, D. Nesterenko, Y. N. Novikov, W. R. Plaß, D. Rodríguez, C. Scheidenberger, L. Schweikhard, P. G. Thirolf, and C. Weber, Science **337**, 1207 (2012).

[4] G. Münzenberg and K. Morita, Nucl. Phys. A **944**, 3 (2015).

[5] G. Münzenberg, Nucl. Phys. A **944**, 5 (2015).

[6] K. Morita, Nucl. Phys. A **944**, 30 (2015).

[7] Y. Oganessian and V. Utyonkov, Nucl. Phys. A **944**, 62 (2015).

[8] J. M. Gates, G. K. Pang, J. L. Pore, K. E. Gregorich, J. T. Kwarsick, G. Savard, N. E. Esker, M. KireeffCovo, M. J. Mogannam, J. C. Batchelder, D. L. Bleuel, R. M. Clark, H. L. Crawford, P. Fallon, K. K. Hubbard, A. M. Hurst, I. T. Kolaja, A. O. Macchiavelli, C. Morse, R. Orford, L. Phair, and M. A. Stoyer, Phys. Rev. Lett. **121**, 222501 (2018).

[9] M. Block, D. Ackermann, D. Beck, K. Blaum, M. Breitenfeldt, A. Chauduri, A. Doemer, S. Eliseev, D. Habs, S. Heinz, F. Herfurth, F. P. Heßberger, S. Hofmann, H. Geissel, H. J. Kluge, V. Kolhinen, G. Marx, J. B. Neumayr, M. Mukherjee, M. Petrick, W. Plass, W. Quint, S. Rahaman, C. Rauth, D. Rodríguez, C. Scheidenberger, L. Schweikhard, M. Suhonen, P. G. Thirolf, Z. Wang, C. Weber, and the SHIPTRAP Collaboration, Eur. Phys. J. A **25**, 49 (2005).

[10] M. Block, Radiochim. Acta **107**, 603 (2019).

[11] S. Eliseev, K. Blaum, M. Block, C. Droese, M. Goncharov, E. Minaya Ramirez, D. A. Nesterenko, Y. N. Novikov, and L. Schweikhard, Phys. Rev. Lett. **110**, 082501 (2013).

[12] D. Rodríguez, Appl. Phys. B **107**, 1031 (2012).

[13] S. Lohse, J. Berrocal, M. Block, S. Chemarev, J. M. Cornejo, J. G. Ramírez, and D. Rodríguez, Rev. Sci. Instrum. **90**, 063202 (2019).

[14] A. Hamaker, G. Bollen, M. Eibach, C. Izzo, D. Puentes, M. Redshaw, R. Ringle, R. Sandler, S. Schwarz, and I. Yandow, Hyperfine Interact. **240**, 34 (2019).

[15] M. J. Gutiérrez, J. Berrocal, J. M. Cornejo, F. Domínguez, J. J. Del Pozo, I. Arrazola, J. Bañuelos, P. Escobedo, O. Kaleja, L. Lamata, R. A. Rica, S. Schmidt, M. Block, E. Solano, and D. Rodríguez, New J. Phys. **21**, 023023 (2019).

[16] E. G. Myers, Atoms **7**, 37 (2019).

[17] D. A. Nesterenko, S. Eliseev, K. Blaum, M. Block, S. Chenmarev, A. Dörr, C. Droese, P. E. Filianin, M. Goncharov, E. Minaya Ramirez, Y. N. Novikov, L. Schweikhard, and V. V. Simon, Phys. Rev. C **90**, 042501(R) (2014).

[18] L. S. Brown and G. Gabrielse, Rev. Mod. Phys. **58**, 233 (1986).

[19] R. C. Thompson and D. C. Wilson, Z. Phys. D **42**, 271 (1997).

[20] S. Mavadia, G. Stutter, J. F. Goodwin, D. R. Crick, R. C. Thompson, and D. M. Segal, Phys. Rev. A **89**, 032502 (2014).

[21] E. A. Cornell, K. R. Boyce, D. L. K. Fygenson, and D. E. Pritchard, Phys. Rev. A **45**, 3049 (1992).

[22] S. Rainville, J. K. Thompson, and D. E. Pritchard, Science **303**, 334 (2004).

[23] B. J. Mount, M. Redshaw, and E. G. Myers, Phys. Rev. Lett. **103**, 122502 (2009).

[24] M. Redshaw, J. McDaniel, and E. G. Myers, Phys. Rev. Lett. **100**, 093002 (2008).

[25] G. Gabrielse, A. Khabbaz, D. S. Hall, C. Heimann, H. Kalinowsky, and W. Jhe, Phys. Rev. Lett. **82**, 3198 (1999).

[26] L. S. Brown and G. Gabrielse, Phys. Rev. A **25**, 2423 (1982).

[27] G. Morigi and H. Walther, Eur. Phys. J. D **13**, 261 (2001).

[28] J. W. Eaton, D. Bateman, S. Hauberg, and R. Wehbring, *GNU Octave Version 4.2.1 Manual: A High-Level Interactive Language for Numerical Computations*, 2017, https://octave.org/doc/interpreter/.

[29] S. Jain, Micro-fabricated Penning trap arrays for quantum simulation, Master's thesis, ETH Zürich, 2018.

[30] S. Jain, J. Alonso, M. Grau, and J. Home, arXiv:1812.06755v3 (2019).

[31] E. A. Cornell, R. M. Weisskoff, K. R. Boyce, R. W. Flanagan, G. P. Lafyatis, and D. E. Pritchard, Phys. Rev. Lett. **63**, 1674 (1989).

[32] M. König, G. Bollen, H.-J. Kluge, T. Otto, and J. Szerypo, Int. J. Mass Spectrom. Ion Processes **142**, 95 (1995).

[33] M. Ubieto-Díaz, D. Rodríguez, S. Lukic, S. Nagy, S. Stahl, and K. Blaum, Int. J. Mass Spectrom. **288**, 1 (2009).

[34] F. Domínguez, I. Arrazola, J. Doménech, J. S. Pedernales, L. Lamata, E. Solano, and D. Rodríguez, Sci. Rep. **7**, 8336 (2017).

[35] J. Home, D. Hanneke, J. Jost, D. Leibfried, and D. Wineland, New J. Phys. **13**, 073026 (2011).

[36] J. F. Goodwin, G. Stutter, R. C. Thompson, and D. M. Segal, Phys. Rev. Lett. **116**, 143002 (2016).

[37] D. M. Meekhof, C. Monroe, B. E. King, W. M. Itano, and D. J. Wineland, Phys. Rev. Lett. **76**, 1796 (1996).